

Parameter identification method for a polycrystalline viscoplastic selfconsistent model based on analytical derivatives of the direct model equations

J W Signorelli[†], R E Logé[‡], Y B Chastel[‡] and R A Lebensohn[†]

[†] Instituto de Física Rosario (UNR-CONICET), 27 de Febrero 210 Bis, 2000 Rosario, Argentina

[‡] École des Mines de Paris, CEMEF, BP 207, 06904 Sophia Antipolis, France

Received 28 September 1999, accepted for publication 31 January 2000

Abstract. An inverse method for automatic identification of the parameters involved in a polycrystalline viscoplastic selfconsistent (VPSC) model is presented. The parameters of the constitutive viscoplastic law at the single-crystal level, i.e. the critical resolved shear stresses (CRSS) of slip and twinning and the micro-hardening coefficients, can be identified using experimental data at the polycrystal level, i.e. stress–strain curves and deformation-induced textures. The minimization problem is solved by means of a Gauss–Newton scheme and the sensitivity matrix is evaluated by analytical differentiation of the direct model equations. As a particular case, the optimization procedure for the Taylor full constraints (FC) formulation is also presented. The convergence and stability of the identification scheme are analysed using several validation tests for different deformation paths imposed to a polycrystal of hexagonal structure. As an example of application of this inverse method, the relative CRSS of the active deformation systems of a Zircaloy-4 sheet are identified, based on several textures measured for different reductions and rolling directions.

(Some figures in this article appear in black and white in the printed version.)

1. Introduction

In recent years, viscoplastic selfconsistent (VPSC) models have been developed in order to describe the mechanical behaviour and the texture evolution of polycrystalline anisotropic materials [1–3]. Different polycrystalline models like the Taylor full constraints (FC) model [4, 5] and the VPSC approach [6–8] have been introduced inside finite element method (FEM) codes in order to account for the evolution of the plastic anisotropy inside each polycrystalline element. Large-scale industrial problems can now be simulated with these coupled FEM–VPSC codes [6], but the results obtained are strongly influenced by the selection of the microscopic (i.e. at a single-crystal level) constitutive parameters of the VPSC model. Usually, these single-crystal constitutive parameters cannot be measured directly, but they must be estimated by indirect methods. This is especially the case for most of the Zr alloys used by the nuclear industry for which the growth of single crystals is extremely difficult. Therefore, the constitutive parameters of these materials, such as critical resolved shear stresses (CRSS) of slip and twinning systems, microscopic rate sensitivity or micro-hardening coefficients, cannot be measured directly. A systematic determination of these parameters, therefore, requires an optimization scheme to find the set of values that gives the best possible agreement between the model predictions and the experimental data available on the mechanical behaviour and the deformation texture development of a given material.

In this work we present an inverse method for the automatic identification of the microscopic constitutive parameters involved in the VPSC model. The solution of such an inverse problem consists of finding the set of parameters that minimizes the difference between the model predictions and the available experimental results [9–11]. This difference is computed by means of a cost function. This function is defined as a weighted summation of the deviations of the model predictions from the corresponding experimental data. In order to perform an automatic optimization, an iterative Gauss–Newton algorithm is used [12]. This algorithm updates the model parameters using a sensitivity matrix, which is defined by the derivatives of the predicted observable quantities with respect to the parameters to be identified. In the present formulation, these derivatives are calculated by analytical differentiation of the direct model equations. As a particular case, we also present a similar optimization procedure for the Taylor FC formulation.

The paper is organized as follows. In section 2, the main equations of the direct VPSC model are reviewed. In section 3, the implementation of the inverse Taylor FC and VPSC models and the strategy for parameter identification are described. In section 4, the convergence and stability of the identification scheme is tested by defining the cost function in terms of theoretical textures calculated using the direct VPSC model, in the case of hcp material deforming by slip and twinning. In section 5, the inverse method is applied for the identification of the CRSS of a Zircaloy-4 (Zrly-4) sheet.

2. Direct model

Unlike the Taylor FC model for which the local strains in the grains are considered to be equal to the macroscopic strain applied to the polycrystal, the VPSC formulation allows each grain to deform differently, according to its directional properties and depending on the strength of the interaction between the grain and its surroundings. In this sense, each grain is in turn considered as an ellipsoidal inclusion surrounded by a homogeneous effective medium (HEM), which has the average properties of the polycrystal. The interaction between the inclusion and the HEM is solved by means of the Eshelby formalism [13]. The HEM properties are not known in advance, but have to be calculated as the average of the individual grain behaviours, once convergence is achieved. Here we present the main equations of the direct VPSC model that are needed to formulate the inverse problem. An exhaustive presentation and discussion of the VPSC formulation can be found in [2].

The polycrystalline aggregate is represented by a set of discrete orientations (hereafter also denoted as grains or single crystals) characterized by three Euler angles and a weight associated with the corresponding volume fraction of material in that orientation. At grain level, slip and twinning are the available deformation modes, while other mechanisms related to diffusion or grain boundary sliding are not taken into account in the present formulation. Each deformation system is characterized by a unit vector $n^{(s)}$ (normal to the slip or twinning plane) and a unit vector $b^{(s)}$ (Burgers vector in the case of slip and twin shear direction in the case of twinning), which allow us to define the Schmid tensor $m^{(s)}$ as:

$$m^{(s)} = \frac{1}{2}(n^{(s)} \otimes b^{(s)} + b^{(s)} \otimes n^{(s)}). \quad (1)$$

The viscoplastic behaviour can be described by a power law relating the applied shear stress on a slip (or twinning) system (s) to the shear rate $\dot{\gamma}^{(s)}$ in the slip (or twinning) direction:

$$\dot{\gamma}^{(s)} = \dot{\gamma}_0 \left| \frac{\tau_r^{(s)}}{\tau_c^{(s)}} \right|^{n-1} \frac{\tau_r^{(s)}}{\tau_c^{(s)}} = \dot{\gamma}_0 \left| \frac{m^{(s)} : \sigma^{lc}}{\tau_c^{(s)}} \right|^{n-1} \frac{m^{(s)} : \sigma^{lc}}{\tau_c^{(s)}} \quad (2)$$

where $\dot{\gamma}_0$ is a reference rate, σ^{lc} is the deviatoric stress in crystal (c), $\tau_c^{(s)}$ is the current CRSS

of system (s) and the exponent n is the inverse of the microscopic rate sensitivity associated with system (s). The strain rate in the single crystal is given by the sum of all the contributions of the potentially active slip and twinning systems:

$$\dot{\epsilon}^c = \sum_s m^{(s)} \dot{\gamma}^{(s)} = \dot{\gamma}_0 \sum_s m^{(s)} \left| \frac{m^{(s)} : \sigma'^c}{\tau_c^{(s)}} \right|^{n-1} \frac{m^{(s)} : \sigma'^c}{\tau_c^{(s)}} \quad (3)$$

which can be written in a pseudo-linear form:

$$\dot{\epsilon}^c = \left\{ \dot{\gamma}_0 \sum_s \frac{m^{(s)} \otimes m^{(s)}}{\tau_c^{(s)}} \left| \frac{m^{(s)} : \sigma'^c}{\tau_c^{(s)}} \right|^{n-1} \right\} : \sigma'^c = M^{c^{sec}}(\sigma'^c) : \sigma'^c \quad (4)$$

where $M^{c^{sec}}$ is the secant viscoplastic compliance tensor that relates the microscopic deviatoric stress tensor and the strain-rate tensor. Another possible linearization of the single-crystal behaviour can be performed by means of a Taylor expansion of expression (4) in terms of the tangent modulus $M^{c^{tg}}$ and a back-extrapolated term $\dot{\epsilon}^0$:

$$\dot{\epsilon}^c = M^{c^{tg}}(\sigma'^c) : \sigma'^c + \dot{\epsilon}^0(\sigma'^c). \quad (5)$$

Similarly, the polycrystal response can be expressed in terms of the overall secant or tangent viscoplastic compliance tensors, which relate the macroscopic strain rate and deviatoric stress:

$$\dot{E} = M^{sec}(\Sigma') : \Sigma' \quad (6)$$

$$\dot{E} = M^{tg}(\Sigma') : \Sigma' + \dot{E}^0(\Sigma'). \quad (7)$$

If the microscopic rate sensitivity is unique (i.e. the same exponent n for every deformation system in every grain), the tangent and secant compliance tensors are proportional to each other at both microscopic and macroscopic [14] levels:

$$M^{c^{tg}} = n M^{c^{sec}} \quad (8)$$

$$M^{tg} = n M^{sec}. \quad (9)$$

The interaction equation relates the differences between the micro and the macro strain rates and deviatoric stresses, as follows:

$$\dot{\epsilon}^c - \dot{E} = -\tilde{M} : (\sigma'^c - \Sigma') \quad (10)$$

where \tilde{M} is the interaction tensor, explicitly given by:

$$\tilde{M} = n(I - S)^{-1} : S : M^{sec} \quad (11)$$

where I is the fourth-order identity tensor and S is the viscoplastic Eshelby tensor, a function of the shape of the inclusion and the macroscopic viscoplastic tangent modulus.

Starting from an initial guess, the macroscopic secant modulus M^{sec} can be adjusted iteratively using the following self-consistent equation:

$$M^{sec} = \langle M^{c^{sec}} : B^c \rangle \quad (12)$$

where $\langle \rangle$ denotes a weighted average over all the grains in the polycrystal and B^c is the accommodation tensor, given for each single crystal by:

$$B^c = (M^{c^{sec}} + \tilde{M})^{-1} : (M^{sec} + \tilde{M}). \quad (13)$$

The accommodation tensor relates the microscopic and macroscopic deviatoric stresses:

$$\sigma'^c = B^c : \Sigma' \quad (14)$$

and therefore

$$\langle B^c \rangle = I. \quad (15)$$

After each strain increment, once convergence is achieved, the reorientation of the grains due to slip and twinning should be performed. If only slip is active, the lattice rotation rate for each grain is given by:

$$\dot{\omega} = \dot{\Omega} - \dot{\omega}^p + \dot{\omega}^e \quad (16)$$

where $\dot{\Omega}$ is the macroscopic rotation rate, $\dot{\omega}^p$ is the skewsymmetric part of the plastic distortion rate due to slip and $\dot{\omega}^e$ is related to the rotation of the ellipsoid representative of the grain. The explicit expressions for $\dot{\omega}^p$ and $\dot{\omega}^e$ are:

$$\dot{\omega}^p = \sum_s \frac{1}{2} (n^{(s)} \otimes b^{(s)} - b^{(s)} \otimes n^{(s)}) \dot{\gamma}^{(s)} \quad (17)$$

$$\dot{\omega}^e = \Pi : S^{-1} : (\dot{\epsilon}^c - \dot{E}) \quad (18)$$

where Π is the skewsymmetric Eshelby rotation tensor [2].

Texture updating during a VPSC calculation can be performed in two different ways. The classical scheme consists of letting each orientation evolve after each time increment Δt , according to the rotation calculated as $\dot{\omega} \Delta t$ (with $\dot{\omega}$ prescribed by equation (16)), while the weights associated with each orientation remain fixed. The other possible scheme is called volume fraction transfer (VFT) [15] and is used in this work in connection with the inverse formulation. Within the VFT scheme, the polycrystal is represented by means of a set of fixed orientations, while the weights are allowed to evolve after each time increment. The Euler space is partitioned regularly into cells of 10° by side. The orientations of the representative grains are made to coincide with the centre of the cells. When plastic deformation is imposed on these grains, the resulting orientations can be regarded as rigid displacements of the cells as a whole. When displaced, the cell partially overlaps with other cells and the volume fraction of material contained in the overlapped portions are transferred to the corresponding cells. The VFT scheme described above is applicable to both slip and twinning reorientation (for details see [15]).

3. Inverse model

3.1. General formulation

The identification of parameters by inverse analysis can be performed by solving a minimization problem. The procedure can be written in the classical form:

$$\text{find } \hat{p} / Q(\bar{C}^{\text{cal}}(\hat{p}), \bar{C}^{\text{exp}}) = \min_{\bar{p} \in P} Q(\bar{C}^{\text{cal}}(\bar{p}), \bar{C}^{\text{exp}}) \quad (19)$$

where $\bar{p} = \{p_1, \dots, p_{N_{\text{par}}}\}$ is the parameter vector, N_{par} is the number of parameters to be identified and the parameter space P is defined by the physically admissible set of values. $\bar{C}^{\text{exp}} = \{C_1^{\text{exp}}, \dots, C_{N_{\text{ob}}}^{\text{exp}}\}$ is the vector of experimental measurements (i.e. observable quantities), N_{ob} is the total number of these observable quantities and $\bar{C}^{\text{cal}}(p) = \{C_1^{\text{cal}}, \dots, C_{N_{\text{ob}}}^{\text{cal}}\}$ is the vector of the analogous model predictions, obtained with a given set of parameters p .

Identification problems are usually formulated as a sequence of three steps: (1) definition of the cost function Q which should express a ‘distance’ between simulated and experimental data; (2) evaluation of the sensitivity matrix for the selected cost function; and (3) minimization of the cost function. In most cases, the cost function is defined as a weighted least square expression:

$$Q = \sum_{i=1}^{N_{\text{ob}}} \beta_i [C_i^{\text{cal}}(\bar{p}) - C_i^{\text{exp}}]^2 \quad (20)$$

where β_i are weighting factors. In the present case the measured data can be deformation textures and/or stress–strain curves for different deformation processes. For better accuracy of the identification method, the Q function should take into account not only the final but also the intermediate crystallographic textures:

$$Q = \sum_{\text{proc}}^{\text{Nproc}} \left[w^{\text{text}} \sum_{\text{text}}^{\text{Ntext}} \sum_i^{\text{Nob}^{\text{text}}} \beta_i^{\text{text}} (C_i^{\text{cal}} - C_i^{\text{exp}})^2 + w^{\text{mech}} \sum_i^{\text{Nob}^{\text{mech}}} \beta_i^{\text{mech}} (C_i^{\text{cal}} - C_i^{\text{exp}})^2 \right]. \quad (21)$$

In (21), Nproc is the number of different deformation processes to be considered in the optimization procedure, Ntext is the number of intermediate and final textures to be considered in each process and Nob^{text} and Nob^{mech} are the numbers of individual observations needed to define a single texture and a single stress–strain curve, respectively. The first and second terms account for the differences between the measured and predicted textures and stress–strain behaviour, respectively. The numbers w^{text} , w^{mech} , β_i^{text} and β_i^{mech} are appropriate factors which define the relative weight of each set of observable quantities.

An iterative algorithm is used to solve the non-linear problem given by expression (19). The cost function Q is minimized using the Gauss–Newton method in combination with a linear search to find the optimal direction and magnitude of a correction vector, at each iteration step. The gradient of the cost function reads:

$$\nabla Q_r(\bar{p}) = \sum_o^{\text{Nob}} 2\beta_i (C_i^{\text{cal}}(\bar{p}) - C_i^{\text{exp}}) \frac{dC_i^{\text{cal}}(\bar{p})}{dp_r}. \quad (22)$$

The Hessian H is given by:

$$H_{rs} = \nabla \otimes \nabla Q(\bar{p}) = \sum_i^{\text{Nob}} 2\beta_i \frac{dC_i^{\text{cal}}(\bar{p})}{dp_r} \frac{dC_i^{\text{cal}}(\bar{p})}{dp_s} + 2\beta_i (C_i^{\text{cal}}(\bar{p}) - C_i^{\text{exp}}) \frac{d^2 C_i^{\text{cal}}(\bar{p})}{dp_r dp_s}. \quad (23)$$

To evaluate the Hessian, both the first- and second-order derivatives of $C_i^{\text{cal}}(\bar{p})$ are required. Neglecting the second-order derivative:

$$H_{rs} \approx \sum_i^{\text{Nob}} 2\beta_i \frac{dC_i^{\text{cal}}(\bar{p})}{dp_r} \frac{dC_i^{\text{cal}}(\bar{p})}{dp_s}. \quad (24)$$

When the parameter vector \bar{p} tends to the solution \hat{p} , the difference $(C_i^{\text{cal}}(\bar{p}) - C_i^{\text{exp}})$ tends to a minimum value and the approximate Hessian (24) tends to the exact Hessian (23). The iterative scheme for solving the minimization problem based on a gradient method leads to the following recursive equation:

$$p_r^{(l+1)} = p_r^{(l)} + \alpha^{(l)} H_{rs}^{-1}(\bar{p}^{(l)}) \nabla Q_s(\bar{p}^{(l)}) \quad (25)$$

where the convergence factor $\alpha^{(l)}$ guarantees the condition $Q^{(l+1)} \leq Q^{(l)}$ after iteration (l) and should be determined using a linear search based on the evaluation of the Q function by means of a direct VPSC calculation.

3.2. Evaluation of the sensitivity matrix

In order to implement the iterative scheme given by equation (25), together with equations (22) and (24), it is necessary to evaluate the sensitivity matrix $[dC_i^{\text{cal}}(\bar{p})]/(dp_r)$ with $i = 1, \text{Nob}$ and $r = 1, \text{Npar}$. The measured and predicted observable quantities C_i^{exp} and $C_i^{\text{cal}}(\bar{p})$ are related to the crystallographic texture or to the stress–strain relationship after each deformation increment. For the sake of simplicity, the algorithm will be described considering that the generic cost function is given by expression (20) such that all the observable quantities are

texture related (i.e. $\text{Nob} = \text{Nob}^{\text{text}}$). Moreover, the microscopic parameters to be identified are the initial CRSS of the active deformation modes (i.e. $N_{\text{par}} =$ number of slip and twinning modes). Other parameters like those associated with microscopic hardening or rate sensitivity are assumed to be known in advance. As discussed earlier, a texture predicted using the VFT scheme is given by a set of orientations fixed in Euler space with associated weights that evolve as deformation proceeds. These weights can be taken as textural observable quantities:

$$C_i^{\text{cal}}(\bar{p}) = w_i(\bar{p}). \quad (26)$$

Accordingly, the measured observable quantities C_i^{exp} can be obtained by a direct integration of the experimental orientation distribution function (ODF). The sensitivity matrix is therefore given by:

$$\frac{dC_i^{\text{cal}}(\bar{p})}{dp_r} = \frac{dw_i(\bar{p})}{dp_r}. \quad (27)$$

Considering the weights as functions of the rotation rate associated with each orientation, the derivatives in expression (27) can be calculated using finite differences:

$$\frac{dw_i(\bar{p})}{dp_r} = \frac{w_i(\dot{\omega} + (d\dot{\omega}/dp_r)\Delta p_r) - w_i(\dot{\omega} - (d\dot{\omega}/dp_r)\Delta p_r)}{2\Delta p_r}. \quad (28)$$

Using (16), the derivatives of the rotation rates can be expressed as:

$$\frac{d\dot{\omega}}{dp_r} = \frac{d\dot{\Omega}}{dp_r} + \frac{d\dot{\omega}^e}{dp_r} - \frac{d\dot{\omega}^p}{dp_r}. \quad (29)$$

If the macroscopic velocity gradient is assumed completely imposed and fixed during the deformation process, the first term on the right of expression (29) vanishes:

$$\frac{d\dot{\Omega}}{dp_r} = 0. \quad (30)$$

Taking derivatives of equation (17), the plastic spin derivative reads:

$$\begin{aligned} \frac{d\dot{\omega}^p}{dp_r} = \sum_s \frac{1}{2} \left[\frac{dn^{(s)}}{dp_r} \otimes b^{(s)} + n^{(s)} \otimes \frac{db^{(s)}}{dp_r} - \frac{db^{(s)}}{dp_r} \otimes n^{(s)} - b^{(s)} \otimes \frac{dn^{(s)}}{dp_r} \right] \dot{\gamma}^{(s)} \\ + \frac{1}{2} (n^{(s)} \otimes b^{(s)} - b^{(s)} \otimes n^{(s)}) \frac{d\dot{\gamma}^{(s)}}{dp_r} \end{aligned} \quad (31)$$

where the first term in the right expression can be considered negligible compared with the second one. Indeed, calculations using the direct model show that the former is two or three orders of magnitude lower than the latter. Hence:

$$\frac{d\dot{\omega}^p}{dp_r} \approx \frac{1}{2} (n^{(s)} \otimes b^{(s)} - b^{(s)} \otimes n^{(s)}) \frac{d\dot{\gamma}^{(s)}}{dp_r}. \quad (32)$$

Finally, taking derivatives of equation (18) gives:

$$\frac{d\dot{\omega}^e}{dp_r} = \frac{d\Pi}{dp_r} : S^{-1} : (\dot{\varepsilon}^c - \dot{E}) - \Pi : S^{-1} : \frac{dS}{dp_r} : S^{-1} : (\dot{\varepsilon}^c - \dot{E}) + \Pi : S^{-1} : \frac{d(\dot{\varepsilon}^c - \dot{E})}{dp_r}. \quad (33)$$

To evaluate (32) and (33), the derivatives of the internal variables $d\Pi/dp_r$, dS/dp_r , $d\dot{\gamma}^{(s)}/dp_r$, $d(\dot{\varepsilon}^c - \dot{E})/dp_r$ must be determined. Concerning the first two terms, the algorithm to calculate the derivatives of the Eshelby tensors is described in appendix B. On the other hand,

the last two terms can be obtained by taking derivatives of expressions (2) and (3). Neglecting the derivatives of the Schmid tensors with respect to the parameters we get:

$$\frac{d\dot{\gamma}^{(s)}}{dp_r} \approx \dot{\gamma}_0 n \left| \frac{m^{(s)} : \sigma^{rc}}{\tau_c^{(s)}} \right|^{n-1} \left[\frac{m^{(s)}}{\tau_c^{(s)}} : \frac{d\sigma^{rc}}{dp_r} - \frac{m^{(s)} : \sigma^{rc}}{(\tau_c^{(s)})^2} \frac{d\tau_c^{(s)}}{dp_r} \right] \quad (34)$$

$$\frac{d(\dot{\varepsilon}^c - \dot{E})}{dp_r} = \frac{d\dot{\varepsilon}^c}{dp_r} \approx \sum_s m^{(s)} \frac{d\dot{\gamma}^{(s)}}{dp_r}. \quad (35)$$

3.3. Taylor approach

In this case, for each grain (independently from the other grains of the aggregate) it is possible to find a linear system of equations whose solution gives directly the derivatives with respect to the parameters of the local stress tensor, the current CRSS and the single shear rates of each deformation system. To build up this system it is necessary to consider: (a) the microscopic hardening law, which gives the expression of the current CRSS of each system given by:

$$\tau_c^{(s)} = \tau_c^{0(s)} + \sum_{s'} \hat{H}_{ss'} |\dot{\gamma}^{s'}| \Delta t \quad (36)$$

where $\hat{H}_{ss'}$ is the known microscopic hardening matrix and $\tau_c^{0(s)}$ is the initial CRSS of system (s), i.e., each one of the microscopic parameters to be identified; and (b) the strict enforcement of compatibility in the Taylor model that prescribes all local strain rates equal to the macroscopic strain rate. Hence, the derivatives of the local strain rate vanish, i.e.

$$\frac{d\dot{\varepsilon}^c}{dp_r} = 0. \quad (37)$$

Taking derivatives with respect to the parameters in (36), recalling (34), replacing (35) in (37) and bearing in mind that $p_r = \tau_c^{0(r)}$, we obtain the following linear system of equations:

$$\frac{d\tau_c^{(s)}}{dp_r} = \delta_{rs} + \sum_{s'} \hat{H}_{ss'} \text{sign}(\dot{\gamma}^{(s')}) \frac{d\dot{\gamma}^{(s')}}{dp_r} \Delta t \quad (S \text{ equations}) \quad (38a)$$

$$\frac{d\dot{\gamma}^{(s)}}{dp_r} = \dot{\gamma}_0 n \left| \frac{m^{(s)} : \sigma^{rc}}{\tau_c^{(s)}} \right|^{n-1} \left[\frac{m^{(s)}}{\tau_c^{(s)}} : \frac{d\sigma^{rc}}{dp_r} - \frac{m^{(s)} : \sigma^{rc}}{(\tau_c^{(s)})^2} \frac{d\tau_c^{(s)}}{dp_r} \right] \quad (S \text{ equations}) \quad (38b)$$

$$0 = \dot{\gamma}_0 \sum_s m^{(s)} \frac{d\dot{\gamma}^{(s)}}{dp_r} \quad (5 \text{ equations}). \quad (38c)$$

The system (38) consists of $5 + 2S$ equations and the same number of unknowns, where S is the number of deformation systems. The unknowns are the five derivatives of the stress components $d\sigma^{rc}/dp_r$, S derivatives of the current CRSS $d\tau_c^{(s)}/dp_r$ and another S derivatives of the single shear rates $d\dot{\gamma}^{(s)}/dp_r$. The sensitivity matrix is then obtained by replacing the latter in (34) and going back to equations (32), (29) and (28) while recalling that $\dot{\omega}^e = 0$ in the Taylor FC case.

3.4. Self-consistent approach

Unlike the Taylor model, the VPSC formulation does not allow the evaluation of the derivatives with respect to the parameters of the stress and strain rate in each grain independently from the values of these derivatives in the other grains of the aggregate. Indeed, the stress- and strain-rate tensors in each grain are related to the average macroscopic values through the interaction equation (10). In what follows, we describe a specific algorithm to obtain those derivatives.

For the sake of simplicity we consider a case of saturated hardening (i.e. $\hat{H}_{ss'} = 0$). Hence, equation (38a) reads:

$$\frac{d\tau_c^{(s)}}{dp_r} = \delta_{rs}. \quad (39)$$

Taking derivatives in equation (14) gives:

$$\frac{d\sigma^{/c}}{dp_r} = \frac{dB^c}{dp_r} : \Sigma' + B^c : \frac{d\Sigma'}{dp_r}. \quad (40)$$

Using (13) and (6) we obtain:

$$\begin{aligned} \frac{d\sigma^{/c}}{dp_r} = & (M^{c\text{sec}} + \tilde{M})^{-1} : \left[- \left(\frac{dM^{c\text{sec}}}{dp_r} + \frac{d\tilde{M}}{dp_r} \right) : (M^{c\text{sec}} + \tilde{M})^{-1} : (M^{\text{sec}} + \tilde{M}) \right. \\ & \left. + \left(\frac{dM^{\text{sec}}}{dp_r} + \frac{d\tilde{M}}{dp_r} \right) - (M^{\text{sec}} + \tilde{M}) : M^{\text{sec}^{-1}} : \frac{dM^{\text{sec}}}{dp_r} \right] : \Sigma'. \end{aligned} \quad (41)$$

The derivatives of the local compliances and the interaction tensor can be obtained from equations (4) and (11):

$$\begin{aligned} \frac{dM^{c\text{sec}}}{dp_r} = & \dot{\gamma}_0 \sum_s \left[(n-1) \text{sign}(m^{(s)} : \sigma^{/c}) \frac{|m^{(s)} : \sigma^{/c}|^{n-2}}{(\tau_c^{(s)})^n} \left(m^{(s)} : \frac{d\sigma^{/c}}{dp_r} \right) \right. \\ & \left. - n \frac{|m^{(s)} : \sigma^{/c}|^{n-1}}{(\tau_c^{(s)})^{n+1}} \delta_{rs} \right] m^{(s)} \otimes m^{(s)} \end{aligned} \quad (42)$$

$$\frac{d\tilde{M}}{dp_r} = n(I - S)^{-1} : \left[\frac{dS}{dp_r} : (I - S)^{-1} : S : M^{\text{sec}} + \frac{dS}{dp_r} : M^{\text{sec}} + S : \frac{dM^{\text{sec}}}{dp_r} \right]. \quad (43)$$

If the Eshelby tensor derivative dS/dp_r is assumed to be known, equations (41)–(43) can be combined to give the following system of linear equations for each single crystal in the aggregate:

$$A_{ij}^c \frac{d\sigma_j^{/c}}{dp_r} + B_{ijk}^c \frac{dM_{jk}^{\text{sec}}}{dp_r} = D_i^c \quad (i, j, k = 1, 5) \quad (44)$$

where an implicit summation on the repeated subscripts (j) and (k) is assumed. The explicit expressions of matrices A_{ij}^c , B_{ijk}^c and D_i^c are given in appendix A. If C is the number of single crystals in the polycrystal, expression (44) gives $5C$ equations and $5C + 25$ unknowns, i.e., five derivatives of the local stress components $d\sigma_j^{/c}/dp_r$ ($j = 1, 5$) for each single crystal and 25 derivatives of components of the macroscopic compliance $dM_{jk}^{\text{sec}}/dp_r$ ($j, k = 1, 5$).

Another 25 additional equations (without increasing the number of unknowns) can be obtained taking derivatives of equation (15) and using (13), (42) and (43) to give:

$$\begin{aligned} \frac{dM^{\text{sec}}}{dp_r} = & \left\langle (M^{c\text{sec}} + \tilde{M})^{-1} \right\rangle^{-1} \left\langle (M^{c\text{sec}} + \tilde{M})^{-1} : \left[\sum_s \left((n-1) \frac{(m^{(s)} : \sigma^{/c})^{n-2}}{(\tau_c^{(s)})^n} \right) \right. \right. \\ & \times m^{(s)} \otimes m^{(s)} \otimes m^{(s)} : \frac{d\sigma^{/c}}{dp} - \sum_s \left(n \frac{(m^{(s)} : \sigma^{/c})^{n-1}}{(\tau_c^{(s)})^{n+1}} \delta_{rs} \right) \\ & \left. \left. \times m^{(s)} \otimes m^{(s)} + n(I - S)^{-1} : \left(\frac{dS}{dp_r} : (I - S)^{-1} : S : M^{\text{sec}} \right. \right. \right. \\ & \left. \left. \left. + \frac{dS}{dp_r} : M^{\text{sec}} + S : \frac{dM^{\text{sec}}}{dp_r} \right) \right] : (M^{c\text{sec}} + \tilde{M})^{-1} \right\rangle : (M^{\text{sec}} + \tilde{M}) - n(I - S)^{-1} \\ & : \left(\frac{dS}{dp_r} : (I - S)^{-1} : S : M^{\text{sec}} + \frac{dS}{dp_r} : M^{\text{sec}} + S : \frac{dM^{\text{sec}}}{dp_r} \right). \end{aligned} \quad (45)$$

Equation (45) can be written in the following compact form:

$$\sum_c E_{ijk}^c \frac{d\sigma_k^c}{dp_r} + F_{ijkl} \frac{dM_{kl}^{\text{sec}}}{dp_r} = G_{ij} \quad (i, j, k, l = 1, 5) \quad (46)$$

where an implicit summation on the repeated subscripts (k) and (l) is assumed. The explicit expressions of matrices E_{ijk}^c , F_{ijkl} and G_{ij} are given in appendix A.

The linear system composed by expressions (44) and (46), i.e.

$$A_{ij}^c \frac{d\sigma_j^c}{dp_r} + B_{ijk}^c \frac{dM_{jk}^{\text{sec}}}{dp_r} = D_i^c \quad (47a)$$

$$\sum_c E_{ijk}^c \frac{d\sigma_k^c}{dp_r} + F_{ijkl} \frac{dM_{kl}^{\text{sec}}}{dp_r} = G_{ij} \quad (47b)$$

should be solved assuming a certain value of the Eshelby tensor derivative. As a first guess, it can be assumed that S is not a function of the parameters (i.e. $dS/dp_r = 0$). Once the system is solved and therefore the macroscopic compliance derivatives are obtained, an improved estimation of the Eshelby tensor derivatives can be evaluated using the method described in appendix B. This new guess of the Eshelby tensor derivatives is then injected into the system (47). This iterative procedure is repeated until the input and output estimations of the Eshelby tensor derivatives coincide within a certain tolerance. The values obtained after convergence of the grain stress derivatives and the Eshelby tensor derivatives can be used in combination with (34) and (35) to evaluate successively the rotation-rate derivatives (equations (32), (33) and (29)) and the sensitivity matrix (equation (28)).

4. Convergence and stability

As for every optimization scheme, it is necessary to assess the numerical stability and the robustness of the present algorithm when dealing with local minima of the cost function. Here, we do not derive an analytical proof, but the identification method is tested for various cases for which the solution is known *a priori*. Instead of using experimental data as observable quantities, deformation textures were calculated using the direct VPSC model for various deformation paths and for a given set of deformation systems with prescribed values of CRSS.

In order to perform an initial convergence test, let us consider an ideal hcp material ($c/a = 1.59$) having the following active deformation modes: $\{10\bar{1}0\}\langle 1\bar{2}10\rangle$ prismatic slip ($\text{pr}\langle a \rangle$), $\{10\bar{1}0\}\langle 11\bar{2}3\rangle$ pyramidal $\langle c + a \rangle$ slip ($\text{pyr}\langle c + a \rangle$) and $\{10\bar{1}2\}\langle 10\bar{1}1\rangle$ tensile twinning (ttw). The viscoplastic exponent (inverse of the rate sensitivity) is taken as $n = 19$. Starting from an initially random polycrystal, four deformation textures were calculated using $\tau_{\text{py}\langle c+a \rangle} / \tau_{\text{pr}\langle a \rangle} = 4.0$ and $\tau_{\text{ttw}} / \tau_{\text{pr}\langle a \rangle} = 1.5$ as nominal CRSS ratios keeping them fixed throughout the calculation. Four different deformation paths were used: (a) uniaxial tension up to 0.5 Von Mises (VM) equivalent strain, (b) plane-strain compression up to 0.2 VM strain, (c) plane-strain compression up to 0.5 VM strain, and (d) plane-strain compression up to 0.5 VM strain followed by a ‘cross’ plane-strain compression (i.e. the final extension direction corresponds to the initial transverse direction) of 0.2 VM strain. The optimization scheme was tested using the weights of the final deformation textures as observable quantities. Regarding the general expression of the cost function (equation (21)), this means: $w^{\text{text}} = 1$, $w^{\text{mech}} = 0$, $N_{\text{proc}} = 4$ and $N_{\text{text}} = 1$. In order to perform a reliable convergence test, the initial values of the CRSS ratios were taken far enough from the actual values, i.e., $\tau_{\text{py}\langle c+a \rangle} / \tau_{\text{pr}\langle a \rangle} = 1.0$ and $\tau_{\text{ttw}} / \tau_{\text{pr}\langle a \rangle} = 1.0$. Table 1 shows that the convergence was reached

Table 1. Results of a convergence test performed for an ideal, initially random hcp polycrystal. Four theoretical textures obtained for the nominal values of CRSS and for different strain paths were used as observable quantities. In parentheses: number of iterations needed for convergence.

	Initial values	Identified values	Nominal values
$\tau_{py(c+a)}/\tau_{pr(a)}$	1.00	3.99	4.00
$\tau_{ttw}/\tau_{pr(a)}$	1.00	1.50	1.50
Q function	0.59	0.000 19(6)	

Table 2. Results of the second convergence test performed for an ideal, initially random hcp polycrystal. A theoretical texture (plane-strain compression, 0.5 VM strain), obtained for the nominal values of CRSS, was used as the source of observable quantities. The identified values converge to the nominal values for three different initial guesses of CRSS considered in this test. In parentheses: number of iterations needed for convergence.

	Guess No 1		Guess No 2		Guess No 3		Nominal
	Initial	Identified	Initial	Identified	Initial	Identified	
$\tau_{ttw}/\tau_{pr(a)}$	1.00	1.48	2.00	1.49	2.00	1.48	1.50
$\tau_{ctw}/\tau_{pr(a)}$	1.00	2.95	1.00	2.97	4.00	2.95	3.00
Q function	0.57	0.011(10)	1.47	0.011(16)	0.16	0.011(8)	

Table 3. Results of the stability test performed for an ideal, initially random hcp polycrystal. A perturbed theoretical texture (plane-strain compression, 0.5 VM strain), obtained for the nominal values of CRSS, was used as the source of observable quantities. The identified values converge to the nominal values before perturbation. In parentheses: number of iterations needed for convergence.

	Guess No 1		Guess No 2		Nominal before perturbation
	Initial	Identified	Initial	Identified	
$\tau_{ttw}/\tau_{pr(a)}$	1.5000	1.5009	1.0000	1.5094	1.5000
$\tau_{ctw}/\tau_{pr(a)}$	3.0000	3.0018	2.0000	3.0020	3.0000
Q function	0.158 22	0.158 20(2)	0.215 68	0.158 19(8)	

after six iterations and that the identified CRSS values match almost exactly with the nominal values.

A second convergence test has been carried out in order to evaluate the sensitivity of the method to the choice of different initial guesses of the CRSS ratios. Once more, we performed this test for an ideal hcp polycrystal with an initial random texture. In this case, the deformation modes were assumed to be prismatic slip, tensile twinning and $\{11\bar{2}2\}\{11\bar{2}\bar{3}\}$ compressive twinning (ctw). A single theoretical texture of plane-strain compression up to 0.5 VM strain with $\tau_{ttw}/\tau_{pr(a)} = 1.5$ and $\tau_{ctw}/\tau_{pr(a)} = 3.0$ was used to identify the *a priori* known CRSS ratios starting from different initial guesses. The results are shown in table 2, while figure 1 displays the oscillations of the CRSS values until the stagnation condition is reached. The identified values effectively converge to the nominal values for three different initial guesses of CRSS considered in this test.

Experimental measurements always contain a certain level of error or noise. It is therefore interesting to study how an inverse method would perform with perturbed observable data. Such tests are often referred to as stability tests. In order to perform such a test, the former plane-strain compression experimental texture was slightly modified by adding a random perturbation of 5% to the original ODF values. This leads to a cost function of 0.158 22 when evaluated for

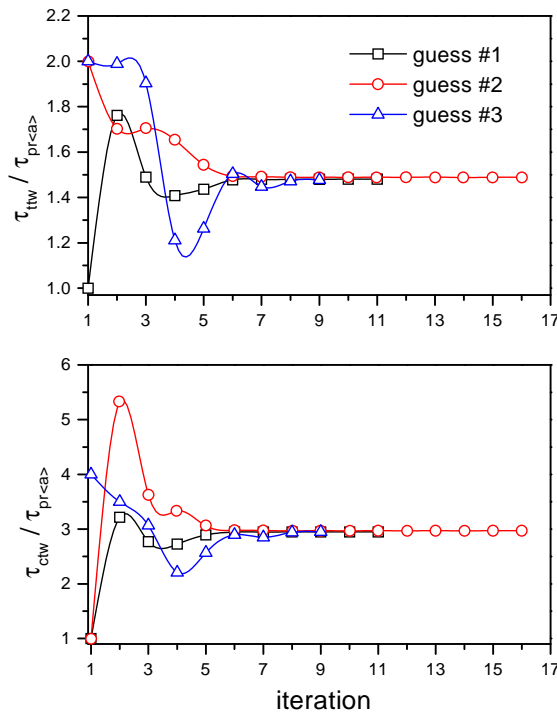


Figure 1. Results of the second convergence test performed for an ideal, initially random hcp polycrystal (see also table 2 caption). Oscillations of the CRSS values, until the stagnation condition is reached.

the original nominal CRSS ratios. Then, the identification scheme was run using the perturbed texture as the source of observable quantities, for a set of initial CRSS ratios equal to the original nominal ratios and another set far enough from the original ratios. Table 3 shows the corresponding results. The perturbation introduced in the original texture does not affect the tendency towards the original nominal values of CRSS for both choices of the initial CRSS ratios, although the value of the cost function after stagnation is one order of magnitude higher than in the non-perturbed cases.

5. Application to zirconium alloys

The inverse VPSC method has been applied to identify the CRSS of the active deformation modes of Zrly-4 deformed at room temperature. Samples cut from a Zrly-4 sheet were rolled in different directions and the textures were measured for different reductions. The initial basal and prismatic pole figures are shown in figure 2. Four textures corresponding to 20 and 50% thickness reduction by rolling along the original rolling direction (direct rolling) and along the original transverse direction (cross rolling) were measured by the x-ray diffraction technique. The measured textures are shown in the left column of figure 3. Each ODF was discretized and all of them were used as observable quantities in the identification procedure.

Different slip and twinning modes have been observed in cold-rolled Zrly-4. Prismatic $\langle a \rangle$ is acknowledged as the softest and therefore the most active deformation mode [16–18]. The activity of $(0001)\langle 1\bar{2}10 \rangle$ basal $\langle a \rangle$ slip (bas $\langle a \rangle$) has also been reported in Zr alloys [16, 19, 20]. On the other hand, the straining of a Zr alloy crystal along its crystallographic $\langle c \rangle$

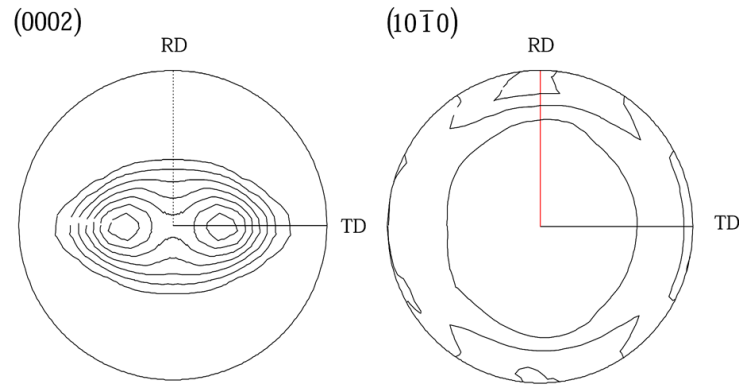


Figure 2. Initial (0002) and (01 $\bar{1}$ 0) pole figures of the Zrly-4 samples. Lines are multiples of random distribution (mrd).

Table 4. Results of the identification procedure for Zrly-4 samples. Four cold-rolling textures (see figure 3, left column) were used as observable quantities. In parentheses: number of iterations needed for convergence.

	Initial values	Identified values
$\tau_{py\langle c+a \rangle} / \tau_{pr\langle a \rangle}$	1.00	5.1
$\tau_{bas\langle a \rangle} / \tau_{pr\langle a \rangle}$	1.00	4.1
Q function	2.003	0.933(4)

Table 5. Results of the identification procedure for Zrly-4 samples including tensile twinning as a potentially active deformation mode. Four cold-rolling textures (see figure 3, left column) were used as observable quantities. In parentheses: number of iterations needed for convergence.

	Initial values	Identified values
$\tau_{py\langle c+a \rangle} / \tau_{pr\langle a \rangle}$	1.00	5.2
$\tau_{bas\langle a \rangle} / \tau_{pr\langle a \rangle}$	1.00	4.3
$\tau_{tw} / \tau_{pr\langle a \rangle}$	1.00	3.6
Q function	2.003	0.921(4)

axis requires the activation of harder modes such as tensile or compressive twinning [17, 18] or pyramidal $\langle c + a \rangle$ slip [18, 21, 22].

In the case of the cold-rolled Zrly-4 samples, very little twinning activity was found [23]. Therefore, as a first attempt, prismatic, basal and pyramidal $\langle c + a \rangle$ were assumed to be the active deformation modes. The parameters to be identified were the CRSS ratios $\tau_{bas\langle a \rangle} / \tau_{pr\langle a \rangle}$ and $\tau_{py\langle c+a \rangle} / \tau_{pr\langle a \rangle}$ which were assumed to remain constant throughout the deformation. The viscoplastic exponent was taken as $n = 19$. The identification procedure was applied to determine the set of CRSS ratios that gives the best simultaneous agreement between the calculated and the measured textures. The results of the identification procedure are shown in table 4 and the calculated textures using the identified CRSS ratios are shown in the right column of figure 3. The final value of the cost function is significantly higher than those obtained in the test cases discussed in section 4. The predicted textures compare acceptably well with the measured values in the direct rolling case, except for a minor component appearing in TD. In the cross-rolling case, the tendency of the basal poles to rotate towards the normal direction (ND) (i.e. in the centre of the pole figure) is not predicted by the model. The simulations

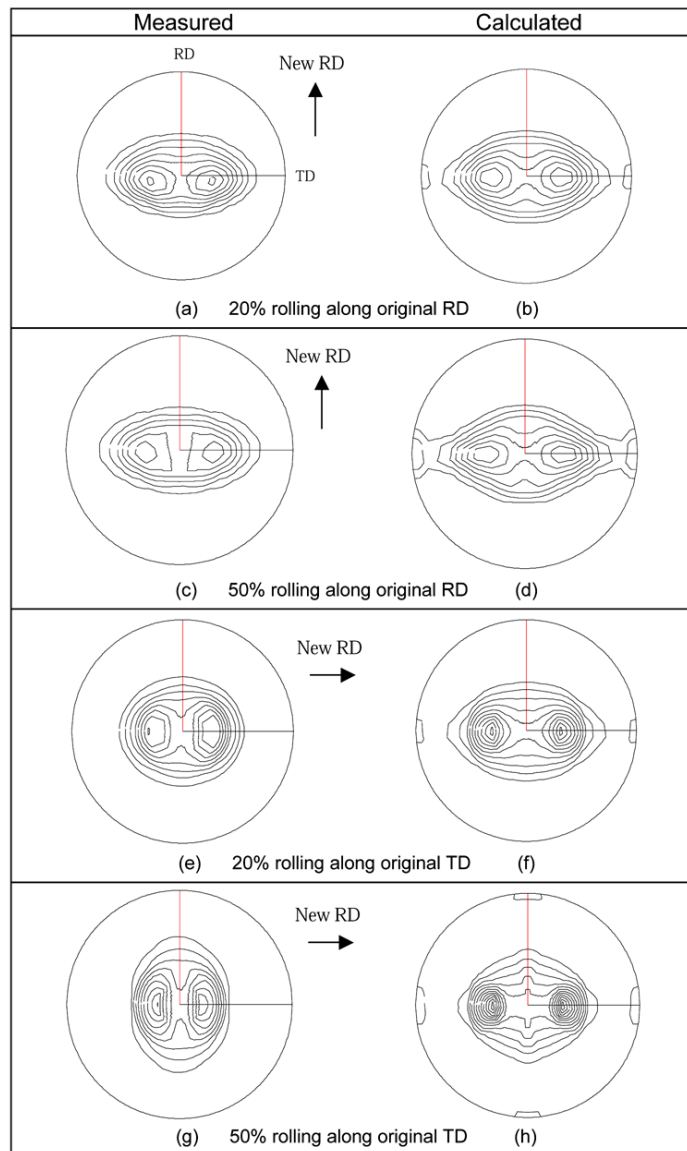


Figure 3. Left: measured (0002) pole figures of cold-rolled Zrly-4 samples for direct rolling at: (a) 20% and (c) 50% thickness reduction and cross rolling at: (e) 20% and (g) 50% thickness reduction. Right: calculated (0002) pole figures with identified parameters for direct rolling at: (b) 20% and (d) 50% thickness reduction and cross rolling at: (f) 20% and (h) 50% thickness reduction. Lines are mrd. The labels RD and TD indicate the original rolling and transverse directions (same for all pole figures), while the arrows indicate the new rolling direction.

show that the basal maxima lying in the original ND–TD plane tend to increase in intensity, but remain in their same original position, at 35° from ND. It is also interesting to analyse the predicted activity of the different deformation modes. In fact, the simulations of both rolling processes performed using the identified CRSS ratios give a relative activity of prismatic slip of the order of 98%, while the remaining 2% corresponds to basal (1.5%) and pyramidal slip

(0.5%).

In the former example only prismatic, basal and pyramidal slip were assumed to be active deformation modes. It is also important to study what would be the identified CRSS ratios if tensile twinning was not *a priori* eliminated from the list of potentially active modes. In this case, three instead of two parameters should be identified: $\tau_{\text{bas}(a)}/\tau_{\text{pr}(a)}$, $\tau_{\text{py}(c+a)}/\tau_{\text{pr}(a)}$ and $\tau_{\text{tw}}/\tau_{\text{pr}(a)}$. All other inputs were identical to the former case. The results of the identification procedure are shown in table 5. If the identified CRSS ratios are used to simulate either direct rolling or the cross rolling, the predicted twinning activity always remains lower than 0.1%. This is consistent with the fact that almost no traces of twinning were found in the rolled samples [23].

6. Conclusion

An inverse method based on the VPSC model for automatic identification of model parameters was presented. In the examples shown in this paper, texture measurements were used as the source of observable quantities and CRSS ratios were the parameters to be identified. However, the present scheme allows us to identify other microscopic constitutive parameters, e.g., microscopic hardening or rate sensitivity, etc, using other measurements (besides crystallographic texture) at a polycrystalline level, e.g., stress–strain curves, grain shape distribution or twinning fraction, etc. The present approach is thought to be a useful tool for the analysis of deformation textures of low symmetry materials in which different deformation modes can be activated depending on the imposed deformation conditions.

Acknowledgments

This work was partially supported by the French–Argentine ECOS-SECYT cooperation program (Project A97E02). The authors would like to thank the Cezuy Company and particularly Dr Pierre Barberis for fruitful discussions on cold rolling of Zircaloy-4 sheets.

Appendix A

The explicit expressions of matrices A_{ij}^c , B_{ijk}^c and D_i^c in equation (44) and E_{ijk}^c , F_{ijkl} and G_{ij} in equation (46) are (indices i, j, k, l and m run from 1 to 5):

$$A_{ij}^c = \delta_{ij} + [(M^{\text{csec}} + \tilde{M})^{-1} : M^{*c}]_{ikj} [(M^{\text{csec}} + \tilde{M})^{-1} : (M^{\text{sec}} + \tilde{M}) : \Sigma']_k \quad (\text{A1})$$

$$B_{ijk}^c = [(M^{\text{csec}} + \tilde{M})^{-1} : n(I - S)^{-1} : S]_{ij} [(M^{\text{csec}} + \tilde{M})^{-1} : (M^{\text{sec}} + \tilde{M}) : \Sigma']_k \\ - [(M^{\text{csec}} + \tilde{M})^{-1} : (I + n(I - S)^{-1} : S - M + \tilde{M}) : M^{\text{sec}^{-1}}]_{ij} [\Sigma']_k \quad (\text{A2})$$

$$D_i^c = \left[(M^{\text{csec}} + \tilde{M})^{-1} : \left(\hat{M}^c + n(I - S)^{-1} : \frac{dS}{dp_r} : (I + (I - S)^{-1} : S) : M^{\text{sec}} \right) \right. \\ \left. : (M^{\text{csec}} + \tilde{M})^{-1} : (M^{\text{sec}} + \tilde{M}) : \Sigma' \right]_i \\ + \left[(M^{\text{csec}} + \tilde{M})^{-1} : n(I - S)^{-1} : \frac{dS}{dp_r} : (I + (I - S)^{-1} : S) : M^{\text{sec}} : \Sigma' \right]_i \quad (\text{A3})$$

$$E_{ijk}^c = -w^c [(M^{\text{csec}} + \tilde{M})^{-1}]_{il} [(M^{\text{csec}} + \tilde{M})^{-1} : M^{*c}]_{lmj} [(M^{\text{csec}} + \tilde{M})^{-1} : (M^{\text{sec}} + \tilde{M})]_{mk} \quad (\text{A4})$$

$$F_{ijkl} = [\langle (M^{\text{csec}} + \tilde{M})^{-1} \rangle^{-1} \langle (M^{\text{csec}} + \tilde{M})^{-1} : n(I - S)^{-1} : S \rangle \otimes \langle (M^{\text{csec}} + \tilde{M})^{-1} : (M^{\text{csec}} + \tilde{M}) \rangle]_{ijkl} - [n(I - S)^{-1} : S]_{ij} \delta_{kl} - \delta_{ij} \delta_{kl} \quad (\text{A5})$$

$$G_{ij} = [\langle (M^{\text{csec}} + \tilde{M})^{-1} \rangle^{-1}]_{ik} \left[\left\langle (M^{\text{csec}} + \tilde{M})^{-1} : \left(\hat{M}^c + n(I - S)^{-1} : \frac{dS}{dp_r} : ((I - S)^{-1} : S + I) : M^{\text{csec}} \right) : (M^{\text{csec}} + \tilde{M})^{-1} : (M^{\text{csec}} + \tilde{M}) \right\rangle \right]_{kj} - \left[n(I - S)^{-1} : \frac{dS}{dp_r} : ((I - S)^{-1} : S + I) : M^{\text{csec}} \right]_{ij} \quad (\text{A6})$$

where:

$$M^{*c} = \sum_s \left((n-1) \frac{(m^{(s)} : \sigma^{lc})^{n-2}}{(\tau_c^{(s)})^n} \right) m^{(s)} \otimes m^{(s)} \otimes m^{(s)} \quad (\text{A7})$$

$$\hat{M}^c = \sum_s \left(n \frac{(m^{(s)} : \sigma^{lc})^{n-1}}{(\tau_c^{(s)})^{n+1}} \delta_{rs} \right) m^{(s)} \otimes m^{(s)}. \quad (\text{A8})$$

Appendix B. Calculation of Eshelby tensor derivatives

The symmetric and skewsymmetric Eshelby tensors of an ellipsoidal inclusion in an anisotropic medium is given by [13]:

$$S_{ijmn} = \Lambda_{ijpq}^S L_{pqmn} \quad (\text{B1})$$

$$\Pi_{ijmn} = \Lambda_{ijpq}^\Pi L_{pqmn} \quad (\text{B2})$$

where L is the stiffness tensor of the medium, expressed in the system of principal axes of the ellipsoid (in the case of the VPSC model L is the inverse of the macroscopic tangent compliance M^{tg}) and Λ^S and Λ^Π are tensors expressed as:

$$\Lambda_{ijpq}^S = \frac{1}{16\pi} \int_0^\pi \sin \theta \int_0^{2\pi} \lambda_{ijpq}^S d\phi \quad (\text{B3})$$

$$\Lambda_{ijpq}^\Pi = \frac{1}{16\pi} \int_0^\pi \sin \theta \int_0^{2\pi} \lambda_{ijpq}^\Pi d\phi \quad (\text{B4})$$

where:

$$\Lambda_{ijpq}^S = [U]_{ip}^{-1}(\zeta) \zeta_j \zeta_q + [U]_{jp}^{-1}(\zeta) \zeta_i \zeta_q + [U]_{iq}^{-1}(\zeta) \zeta_j \zeta_p + [U]_{jq}^{-1}(\zeta) \zeta_i \zeta_p \quad (\text{B5})$$

$$\Lambda_{ijpq}^\Pi = [U]_{ip}^{-1}(\zeta) \zeta_j \zeta_q - [U]_{jp}^{-1}(\zeta) \zeta_i \zeta_q + [U]_{iq}^{-1}(\zeta) \zeta_j \zeta_p - [U]_{jq}^{-1}(\zeta) \zeta_i \zeta_p \quad (\text{B6})$$

and where U is a symmetric tensor defined by:

$$U_{ip}(\zeta) = L_{ijpl} \zeta_j \zeta_l \quad (\text{B7})$$

with:

$$\zeta_1 = \frac{\sin \theta \cos \phi}{a_1}, \quad \zeta_2 = \frac{\sin \theta \sin \phi}{a_2}, \quad \zeta_3 = \frac{\cos \theta}{a_3} \quad (\text{B8})$$

where a_1, a_2, a_3 are the lengths of the ellipsoid's principal axes and where the angles ϕ and θ ($0 < \phi < 2\pi$ and $0 < \theta < \pi$) are the spherical coordinates defining the vector ζ .

Taking derivatives of equations (B1) and (B2) with respect to a parameter p_r gives:

$$\frac{dS_{ijmn}}{dp_r} = \frac{d\Lambda_{ijpq}^S}{dp_r} L_{pqmn} + \Lambda_{ijpq}^S \frac{dL_{pqmn}}{dp_r} \quad (\text{B9})$$

$$\frac{d\Pi_{ijmn}}{dp_r} = \frac{d\Lambda_{ijpq}^\Pi}{dp_r} L_{pqmn} + \Lambda_{ijpq}^\Pi \frac{dL_{pqmn}}{dp_r}. \quad (\text{B10})$$

The first terms in (B9) and (B10) are given by:

$$\frac{d\Lambda_{ijpq}^S}{dp_r} = \frac{1}{16\pi} \int_0^\pi \sin \theta \int_0^{2\pi} \frac{d\lambda_{ijpq}^S}{dp_r} d\phi \quad (\text{B11})$$

$$\frac{d\Lambda_{ijpq}^\Pi}{dp_r} = \frac{1}{16\pi} \int_0^\pi \sin \theta \int_0^{2\pi} \frac{d\lambda_{ijpq}^\Pi}{dp_r} d\phi \quad (\text{B12})$$

with:

$$\frac{d\lambda_{ijpq}^S}{dp_r} = \frac{d[U]_{ip}^{-1}(\zeta)}{dp_r} \zeta_j \zeta_q + \frac{d[U]_{jp}^{-1}(\zeta)}{dp_r} \zeta_i \zeta_q + \frac{d[U]_{iq}^{-1}(\zeta)}{dp_r} \zeta_j \zeta_p + \frac{d[U]_{jq}^{-1}(\zeta)}{dp_r} \zeta_i \zeta_p \quad (\text{B13})$$

$$\frac{d\lambda_{ijpq}^\Pi}{dp_r} = \frac{d[U]_{ip}^{-1}(\zeta)}{dp_r} \zeta_j \zeta_q - \frac{d[U]_{jp}^{-1}(\zeta)}{dp_r} \zeta_i \zeta_q + \frac{d[U]_{iq}^{-1}(\zeta)}{dp_r} \zeta_j \zeta_p - \frac{d[U]_{jq}^{-1}(\zeta)}{dp_r} \zeta_i \zeta_p \quad (\text{B14})$$

where:

$$\frac{dU_{ip}(\zeta)}{dp_r} = \frac{dL_{ijpl}}{dp_r} \zeta_j \zeta_l. \quad (\text{B15})$$

The Eshelby tensors and their derivatives can be directly evaluated by numerical integration. In the VPSC case, if the macroscopic tangent compliance and its derivatives are known, the stiffness tensor derivatives can be calculated as follows:

$$\frac{dL}{dp_r} = -M^{\text{tg}^{-1}} : \frac{dM^{\text{tg}}}{dp_r} : M^{\text{tg}^{-1}}. \quad (\text{B16})$$

References

- [1] Molinari A, Canova G R and Ahzi S 1987 A selfconsistent approach of the large deformation polycrystal viscoplasticity *Acta Metall.* **35** 2983–94
- [2] Lebensohn R A and Tomé C N 1993 A self-consistent approach for the simulation of plastic deformation and texture development of polycrystals: application to Zr alloys *Acta Metall. Mater.* **41** 2611–24
- [3] Lebensohn R A and Canova G R 1997 A selfconsistent approach for modelling texture development of two-phase polycrystals: application to Ti alloys *Acta Mater.* **45** 3687–94
- [4] Beaudoin A J, Mathur K K, Dawson P R and Johnson G C 1993 Three-dimensional deformation process simulation with explicit use of polycrystal plasticity models *Int. J. Plast.* **9** 833–60
- [5] Beaudoin A J, Dawson P R, Mathur K K and Kocks U F 1995 A hybrid finite element formulation for polycrystal plasticity with consideration of macrostructural and microstructural linking *Int. J. Plast.* **11** 501–21
- [6] Logé R, Signorelli J W, Lebensohn R A, Chastel Y and Barberis P 1998 Modeling anisotropic evolution in sheet metal forming using a viscoplastic polycrystalline self-consistent model coupled with a 3D finite element code *Simulation of Material Processing: Theory, Methods and Applications (NUMIFORM'98)* ed J Huétink and F P T Baaijens (Rotterdam: Balkema) pp 329–34
- [7] Maudlin P, Tomé C N, Kaschner G and Gray G 1998 Introduction of polycrystal constitutive laws in a finite element code with application to zirconium forming *Simulation of Material Processing: Theory, Methods and Applications (NUMIFORM'98)* ed J Huétink and F P T Baaijens (Rotterdam: Balkema) pp 309–13
- [8] Tomé C N, Maudlin P J, Lebensohn R A, Kaschner G C and Bingert J F 2000 Describing the constitutive response of zirconium inside finite element codes by means of a polycrystal approach *Acta Mater.* submitted
- [9] Tikhonov A and Arsenine V 1974 *Methodes de resolution de problemes mal poses* (Moscou: Mir)
- [10] Tortorelli D and Michaleris P 1994 Design sensitivity analysis: overview and review. *Inverse Problems in Engineering* **1** 71–105
- [11] Cailletaud G and Pilvin P 1993 Identification, problemes inverses: un concept modulaire *Actes du Colloque National en Calcul des Structures* pp 770–87
- [12] Gill P, Murray W and Wright M 1981 *Practical Optimization* (London: Academic)
- [13] Mura T 1988 *Micromechanics of Defects in Solids* (Dordrecht: Martinus-Nijhoff)
- [14] Hutchinson J W 1976 Bounds and selfconsistent estimates for creep of polycrystalline materials *Proc. R. Soc. A* **348** 101–29

- [15] Tomé C N, Lebensohn R A and Kocks, U F 1991 A model for texture development dominated by deformation twinning: application to Zr alloys *Acta Metall. Mater.* **39** 2667–80
- [16] Akhtar A 1973 Basal slip in zirconium *Acta Metall.* **21** 1–8
- [17] Tenckhoff E 1978 The development of the deformation texture in Zr during sequential rolling passes *Metall. Trans. A* **9** 1401–12
- [18] Tenckhoff E 1974 Operable deformation systems and mechanical behaviour of textured Zircaloy tubing *Zirconium in Nuclear Applications ASTM STP* **551** 179–91
- [19] Philippe M J, Serghat M, Van Houtte P and Esling C 1995 Modeling of texture evolution for materials of hexagonal symmetry. II—Application to zirconium and titanium alpha-alloys or near-alpha-alloys *Acta Metall. Mater.* **43** 1619–30
- [20] Fundenberger J J, Philippe M J, Wagner F and Esling C 1997 Modelling and prediction of mechanical properties for materials with hexagonal symmetry (zinc, titanium and zirconium alloys) *Acta Mater.* **45** 4041–55
- [21] Pochettino A, Gannio, N, Vial C and Penelle R 1992 Texture and pyramidal slip in Ti, Zr and their alloys *Scripta Metall. Mater.* **27** 1952–8
- [22] Akhtar A 1973 Compression of Zr single crystals parallel to the c-axis *J. Nucl. Mater.* **47** 79–84
- [23] CEZUS Company 1997 Internal report